

High Contrast L' Band Adaptive Optics Imaging to Detect Extrasolar Planets

Ari Heinze, Phil Hinz, Suresh Sivanandam, Daniel Apai, and Michael Meyer^a

^aAll authors affiliated with Steward Observatory, University of Arizona, 933 N Cherry Ave, Tucson, AZ, 85721, USA;

ABSTRACT

We are carrying out a survey to search for giant extrasolar planets around nearby, moderate-age stars in the mid-infrared L' and M bands (3.8 and 4.8 microns, respectively), using the Clio camera with the adaptive optics system on the MMT telescope. To date we have observed 7 stars, of a total 50 planned, including GJ 450 (distance about 8.55pc, age about 1 billion years, no real companions detected), which we use as our example here. We report the methods we use to obtain extremely high contrast imaging in L', and the performance we have obtained. We find that the rotation of a celestial object over time with respect to a telescope tracking it with an altazimuth mount can be a powerful tool for subtracting telescope-related stellar halo artifacts and detecting planets near bright stars. We have carried out a thorough Monte Carlo simulation demonstrating our ability to detect planets as small as 6 Jupiter masses around GJ 450. The division of a science data set into two independent parts, with companions required to be detected on both in order to be recognized as real, played a crucial role in detecting companions in this simulation. We mention also our discovery of a previously unknown faint stellar companion to another of our survey targets, HD 133002. Followup is needed to confirm this as a physical companion, and to determine its physical properties.

Keywords: extrasolar planets, adaptive optics, L', high contrast, HD 133002, GJ450

1. INTRODUCTION

Slightly over a decade ago, the observational science of extrasolar planetary systems began with the discovery of the planet 51 Pegasi B by Michel Mayor and Didier Queloz. Since that time nearly 200 additional extrasolar planets have been discovered, mostly by using precise spectroscopic radial velocity measurements to detect the reflex motion of the parent star in response to the orbiting planet's gravity – the same method used in the 51 Pegasi detection. Direct imaging of extrasolar planets remains an elusive goal.

It is a very attractive goal, however. A planet detected by direct imaging could be investigated with spectroscopy and multi-band photometry, and astrometric measurements over time would yield its exact orbit. Far more could be learned about such a planet than about one that is only detected by the radial velocity method. Also, the radial velocity method is most sensitive to planets in fairly close-in orbits, unlike the giant planets in our own solar system. Direct imaging is needed to find planets further out, and thus systems more analagous to our own.

Immediately after their formation in the protoplanetary disk of a star, giant planets are extremely hot due to the gravitational potential energy released in their accretion, and therefore glow brightly at infrared wavelengths. Since they have no internal source of energy, they cool over time, and their infrared flux decreases and shifts toward longer wavelengths. Theoretical models¹ show that the current generation of large astronomical telescopes with adaptive optics (AO) systems is capable of directly imaging giant extrasolar planets in the infrared. The cooling properties of extrasolar planets, and the distribution of stars in the sun's vicinity, suggest two good strategies. First, a planet search may focus on very young stars using the near infrared H and K bands (1.6 and 2.2 microns, respectively). Stars with ages in the range of 5-30 million years (Myr) are good targets for this method, because their giant planets will still be bright at short wavelengths. Such searches can detect planetary systems that are still in the process of formation – a fascinating possibility. However, stars that are sufficiently

Ari Heinze is the corresponding author. Email aheinze@as.arizona.edu

young are rare, and therefore tend to be distant from the sun, so only bright planets at relatively large physical separations can be detected. A second promising method is to use longer infrared wavelengths, such as the L' and M bands (3.8 and 4.8 microns, respectively) to observe nearer stars at more moderate ages. At these wavelengths, giant planets can be seen around very nearby stars up to the 5 billion year (Gyr) age of our own solar system. Younger stars are still preferred, but excellent sensitivity can be obtained for stars in the 100 Myr to 1 Gyr range, far older than the optimal range for H and K searches. Stars at these ages are far more common than those younger than 100 Myr, and many examples can be found very close to the sun. Very faint planets can be detected around such nearby stars, and planets at small physical separations from their parent stars can be resolved.

We have begun an L' and M band survey of 50 nearby, moderate age stars for extrasolar planets, using the newly developed L' and M band camera Clio on the 6.5 meter MMT telescope of the University of Arizona, with its deformable secondary AO system. We obtain slightly better sensitivity to low-mass planets in the L' band than in the M band, so we plan to do our initial observations in L' and use the M band for followup as needed. To date, we have observed 7 of our 50 survey targets. We present here the methods we use to obtain extremely high contrast and sensitivity. In Section 2 we describe our observations. Section 3 presents our data analysis methods. In Section 4 we give a detailed analysis of the sensitivity we have obtained for planets orbiting the star GJ 450, one of the 7 targets we have observed so far. No companions to GJ 450 have been detected. In Section 5 we announce the discovery of a probable low-mass star orbiting another of our survey targets, HD 133002. Section 6 gives our conclusions.

2. OBSERVATIONS

On the nights of April 10, 11, and 12, 2006, we obtained long L' band integrations on 7 nearby, moderately young stars using the Clio camera with the AO system on the MMT, obtaining an hour of integration or more on every target except one, on which we obtained only 30 minutes. Each integration was composed of tens to hundreds of individual frames, and each frame was a coadded stack of either 10 or 25 individual 2 second exposures. We turned the instrument rotator off, so that the Clio instrument remained fixed with respect to the telescope. Because the MMT is on an altazimuth mount, as it tracks celestial objects they rotate with respect to both the telescope and the instrument. Since our frame times were so short, having the instrument rotator off did not cause any blurring, and the rotation of the celestial objects with respect to the telescope and instrument was an important part of our overall strategy (see Section 3). We observed each target as close to its transit as possible, to maximize this rotation as well as to obtain observations at the lowest airmass.

In order to subtract off glows and other artifacts due to the instrument and telescope, we took our data in nodded pairs. That is, we would take a series (usually 5) frames with the star on one position on the detector, and then move the telescope about 5-8 arcseconds and take another series of images with the star in a different detector position. Then the subtraction of an image in one nod position from an image in another yields an image in which all telescope and instrument artifacts common to both nod positions vanish, and any celestial objects remain. The only disadvantage is the negative image of the star from the other nod position, behind which, of course, nothing can be detected. It is worth this loss of sensitivity in a small area, however, to ensure that images from both nod positions can be used for science, and to achieve this end we always arranged the nod so that the star was well placed on the detector in both nod positions.

With 2 second exposures, the core of the star image was always saturated. In order to obtain an estimate of the full point spread function (PSF) obtained on each target, acquire L' photometry, and monitor the atmospheric transparency, we took 8-60 shorter frames on each target, interspersed among the longer exposures. We used 0.36 or 0.16 second exposure times for these images to avoid saturating the image cores.

The weather was clear during all of our science observations. The seeing, however, was sometimes worse than 1-1.5 arcseconds, and this combined with windshake to broaden our psf core somewhat beyond the nominal diffraction limit in some cases. This reduced the sensitivity slightly, but the data remain very good and suitable for the detection of extrasolar planets.

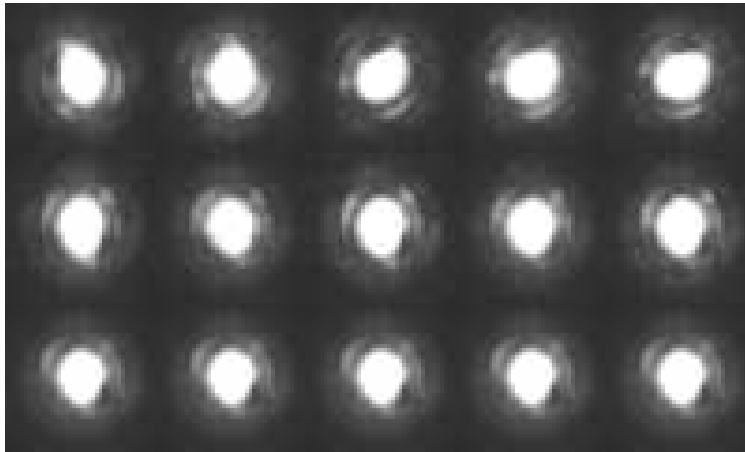


Figure 1. Images showing how the PSF rotates with respect to real celestial objects, but remains fixed with respect to the telescope. The upper row shows images that have been rotated in processing to be fixed with respect to any real sources. The second row shows the same images fixed with respect to the telescope. The bottom row simply shows 5 identical copies of the master PSF image that was constructed for this data set (see Section 3), fixed with respect to the telescope.

3. DATA PROCESSING

The basics of our processing pipeline are dark subtraction; flat fielding; subtraction of nodded pairs of images; noise removal through several types of bad pixel fixing and artifact correction; shifting and rotation of images to move the star to a consistent position on every image, and to remove the effect of the rotation of celestial objects with respect to the instrument; and finally stacking of all the images to produce a master image on which any faint sources can be detected. We produce the master image using a creeping mean combine; that is, if we have n images we therefore have n values for each pixel. For each given pixel, we find the mean of these n values, reject the value farthest from this mean, find the mean of the remainder, reject the value farthest from this mean, etc, until a pre-determined fraction of the values, usually 20 %, have been rejected. This powerfully eliminates artifacts, but real sources, present on every image, are not affected. As our final step in image processing we apply an unsharp mask using a gaussian kernel with $\sigma = 5.0$ pixels, to allow point sources to stand out above the stellar halo.

In the processing, the fact that celestial objects rotate with respect to the telescope and instrument during observations becomes important. Ghosts, rays of scattered light, and other artifacts present in Clio do not rotate with real celestial objects, rather, they remain fixed with respect to the telescope and instrument. Therefore, when the images are rotated in processing to follow real celestial objects, the ghosts are in a different location on each image and vanish on the creeping mean combine. Real sources are not affected.

An additional step in our processing makes further use of the rotation of real objects with respect to the telescope and instrument. All AO systems on large telescopes are plagued with 'super-speckles,' that is, diffraction speckles due to imperfections in the telescope optical surfaces that are not corrected with AO and which, unlike residual atmospheric speckles, change only slowly with time and do not smooth out in long integrations. However, the super speckles remain fixed with respect to the telescope, while real sources rotate. Thus, a stack of images fixed with respect to the telescope may be constructed from a night's data on a particular star, and these may then be creeping-mean combined with high rejection, say 50 %, to create a master PSF image in which only super speckles and artifacts, no real sources, appear. This image may then be subtracted from each individual data frame just prior to rotation in the ordinary processing sequence. Superspeckles are strongly suppressed, but real sources are unaffected. See Figure 1 for a demonstration of superspeckles and image rotation, and Figure 2 for the improvement in sensitivity that results from this processing method. Previous AO observers have used a similar method.²

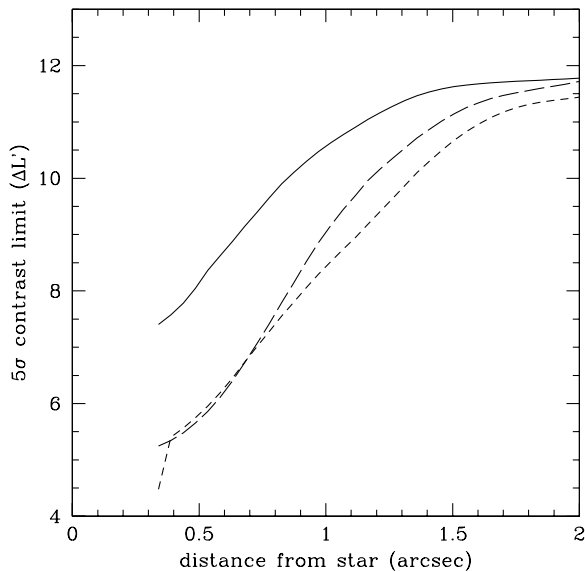


Figure 2. Highest detectable contrast ratio between the star and the planet in magnitudes, as a function of radius in arcseconds, for three different data processing schemes. The short-dashed line is for our basic processing with unsharp masking. The long-dashed line is for radial arc subtraction, and the solid line is for full psf subtraction (see Section 3). Note that we obtain 5σ sensitivity above 10.0 magnitudes, or a factor of 10^4 , at 1.0 arcsecond separation with optimal processing.

4. SENSITIVITY ANALYSIS

After examining our 7 targets, we decided that the star GJ 450 would provide the best example of the typical sensitivity we can obtain. Our science data on this star consists of a 5355 second integration made on the night of April 11, 2006. We analyzed our sensitivity first by obtaining the approximate PSF of any real sources from the unsaturated, short exposure images described in Section 2. We normalized this PSF and then performed a least-square fit for every pixel in our fully processed combined science images, to produce a new image containing the integrated flux of the best-fit PSF centered on each pixel. Our least-squares fit to the PSF template allowed for a variable sky background 'pedestal' under the PSF at each location. The full width at half maximum (FWHM) of our PSF was typically about 3.0 pixels, and we used a fitting radius of 6.0 pixels to ensure that the background level was accurately fit. We then took the image containing the integrated flux of the best-fit PSF at each pixel, and used it to construct an estimate of our 5σ sensitivity limit at each pixel by calculating the rms in a small region surrounding that pixel and then multiplying it by 5. For pixels beyond the halo of the primary star we calculated the rms within a circle of 7-pixel radius, but for pixels within the primary star halo we used instead a 45 pixel long arc at fixed radius from the primary star, centered on the pixel under consideration. We smoothed the resulting sensitivity image with a gaussian kernel of $\sigma = 3.0$ pix, and radially averaged it to produce Figure 2, which presents the 5σ contrast limit for companions at different distances from the star, in the case of our standard processing, an intermediate processing using the subtraction of radial arc-averages, and the full PSF subtraction described in Section 3.

There are so many unknowns in planet detection, so many faint artifacts or noise bursts that can imitate real sources, that no sensitivity analysis is complete without a Monte-Carlo simulation demonstrating ability to detect simulated planets added into real data down to a given threshold. To carry out a Monte-Carlo simulation, we first made an image giving the best 5σ sensitivity limit obtained by any of the three processing methods shown in Figure 2, plus one other which simply involved unsharp masking each individual image before stacking, and smoothed this image as described above. Then, we wrote a code to use this master sensitivity image to insert a random selection of planets of fixed significance level into the raw data. The number, separations, and

position angles of all these planets were randomly chosen within user-specified bounds, and their characteristics were written to a file. We made data sets with simulated planets at significance levels of 10 and 5 σ . Then, without looking at the file containing the planet characteristics, and thus without knowing even the number of planets that had been inserted, we processed the data and tried to identify the inserted planets on the final images. It was immediately obvious that the 5 σ planets could not be confidently detected, and thus our 5 σ sensitivity estimates do not correspond to upper limits on real sources.

We then tried the images with 10 σ planets. Figure 3 shows a final processed version of these images, with full PSF subtraction applied. Several planets are immediately apparent to the eye, but others could not be confidently distinguished from artifacts. We wrote an automated planet detection code based on the method by which we constructed the sensitivity images. A key additional component of this code was that it did not report the detection of a source unless it was found on a master image made from all the science data *and* (albeit at lower significance) on each of two independent master images constructed from the first and second halves of the science data. This requirement was absolutely crucial in order to avoid tens to hundreds of spurious detections. We detected planets on the 10 σ images using this automated detection, and simple examination by eye. Examination by eye allowed us to rule out a few of the automated detections, and to include two other sources which appeared real but had not been automatically detected. Having thus constructed a master list of apparent planets, we looked at the 'secret' file written by our simulated planet code for the first time. We found that 17 simulated planets had been inserted into the data at a 10 σ sensitivity limit. We had found them all, and had made no spurious detections. Our thorough, blind Monte Carlo simulation confirmed our ability to detect 10 σ planets with very high completeness. Figure 4 shows the 10 σ mass limits for planets orbiting GJ 450, as a function of separation in AU, based on theoretical models.¹ Table 1 gives the data on our 17 simulated planets, including their masses again based on theoretical models.¹ These mass sensitivities assume an age of 1 Gyr for GJ 450, which is reasonable based on its X-ray brightness.

5. HD 133002

On the night of April 12, 2006, we obtained a 3500 second L' band integration on the star HD 133002, one of our survey targets. We detected a faint stellar companion at separation 1.8570 ± 0.0037 arcsec, position angle $118.16 \pm 0.15^\circ$, and $L' = 10.87 \pm 0.10$, where approximate 1 σ errors are given.

Our careful internet and literature searches have as yet not turned up any previous mention of this companion, so it appears we have discovered it. Ironically, our searches did indicate that the star HD 133002 should not have been on our target list. We had used the Gliese Catalog parallax for this star, which indicated a distance of 15.38 pc. It now appears that the Gliese parallax is in error, and the true distance to the star from Hipparcos is 43.3 pc. The age also appears to be much larger than we had thought, as high resolution spectroscopy indicates the star is a metal-poor subgiant.³ Simbad records its spectral type as F9. Given our observed L' magnitude of 10.87 ± 0.10 for the companion, and the Hipparcos distance to the system, we find that if the companion is physical its absolute L' magnitude is 7.69 ± 0.10 . An M5 V star has an absolute L' magnitude of 5.71 and a mass of 0.21 solar masses.⁴ The absolute L' magnitude of a star of 0.1 solar masses and age of 1 to 5 Gyr, between which age limits the HD 133002 system probably lies, is about 9.07.¹ Thus the companion mass appears to be between 0.1 and 0.21 solar masses, again assuming the two stars to be physically associated. Assuming a mass for HD 133002 A of 1 solar masses, and that the companion is in a circular orbit at the projected distance, its period is about 700 years. The accuracy of our position and the high proper motion of the system imply a 5 σ proper motion confirmation that the companion is physical will be possible with another measurement of similar accuracy by early June 2006, and orbital motion will likely be detectable in 1-2 years.

6. CONCLUSION

The combination of the Clio L' and M band camera and the MMT AO system is capable of sensitive, high contrast observations in the L' band. Detection of planets in the L' band requires extensive data processing. Our method of using sky rotation to remove super speckles is powerful, at least in the specific case of the MMT and its AO system. Estimating the sensitivity of L' observations in extrasolar planet searches is tricky and very important in order for upper limits to be meaningful. Simple sensitivity estimates based on the rms of

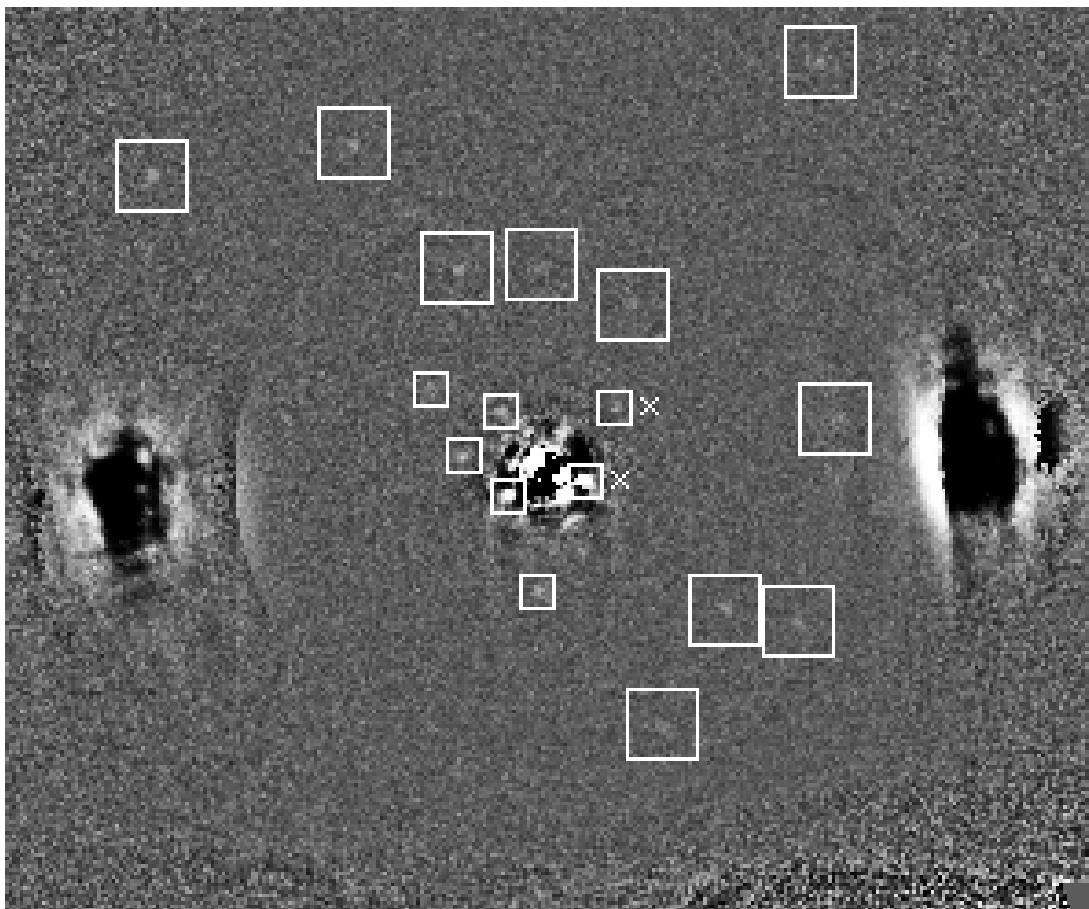


Figure 3. Image of GJ 450 with the 17 simulated 10σ planets of the Monte Carlo simulation inserted. This is a master image made from the entire data set with full PSF subtraction and 20 % creeping mean rejection in the final combine. Large boxes are drawn around the 10 planets that could be confidently detected without PSF subtraction, while small boxes indicate the 7 that required subtraction. Small X's on the right hand side mark the two boxes showing companions that were not detected by the automated code, but were, however, correctly identified manually while still in the blind phase of the simulation. Dark regions to the right and left of the central star are residual negative images from the nod-subtraction.

Table 1. Properties of simulated 10σ planets used in our Monte Carlo simulation. Astrometric error refers to the difference between the true position of the planet as placed by the simulation code, and the position as derived by centroiding on the science images. The errors are impressively low, indicating proper motion confirmation on any real companions we detect can be achieved quickly. Photometric error refers to the true magnitude of the input planet minus that derived from aperture photometry on the science image, with an aperture correction from the unsaturated PSF image. The large negative errors of close-in planets are due to their being partially subtracted away in the PSF subtraction, which is possible because of the particular form of the sky rotation vs time for this star. Our processing will be modified to reduce or eliminate this effect.

Seperation (arcseconds)	Magnitude (L')	Astrometric error (milliarcseconds)	Photometric error (magnitudes)	Mass (M Jup)
0.51	12.53	6.99	-1.17	28.08
0.56	13.32	23.85	-1.07	20.55
0.95	15.35	45.53	-0.73	9.85
1.14	15.6	6.94	-0.46	8.96
1.27	15.96	7.97	-0.83	7.66
1.58	16.06	33.25	-0.18	7.40
1.90	16.51	12.51	-0.28	6.05
2.50	16.59	18.57	-0.38	5.89
2.69	16.57	33.44	-0.42	5.91
2.91	16.38	12.7	0.12	6.44
2.98	16.6	12.89	0.12	5.87
3.71	16.51	18.71	-0.17	6.05
3.90	16.59	29.55	-0.28	5.88
3.93	16.62	8.64	-0.72	5.83
5.02	16.49	19.78	-0.05	6.11
6.52	16.43	23.21	-0.22	6.29
6.53	16.27	27.08	0.1	6.78

image regions should never be trusted without confirmation by Monte Carlo simulation, preferably a carefully constructed blind simulation such as we have carried out. Our simulation demonstrated our ability to detect planets of 6 Jupiter masses orbiting a 1 Gyr old star, and if planets near this mass are sufficiently common in 10-40 AU orbits we will probably discover some of them in the course of our survey. Our method of splitting the data into two independent halves and requiring that any real source be detectable on both halves is a good one in order to sort through numerous spurious detections and find those that are real. The acquisition of a small number of short, unsaturated exposures of our science targets also played an important role in our sensitivity calculation and our Monte Carlo simulation, as it allowed us to accurately know the true PSF a planet would be expected to have.

We have discovered a stellar companion to HD 133002. If it is physically related to HD 133002, it is a low mass red dwarf between 0.1 and 0.21 solar masses. It awaits proper motion confirmation and other followup studies.

ACKNOWLEDGMENTS

We thank Andy Breuninger for many hours spent writing, improving, and testing the software that runs the Clio camera. We also thank MMT telescope operators John McAfee and Michael Alegria, and AO system operators

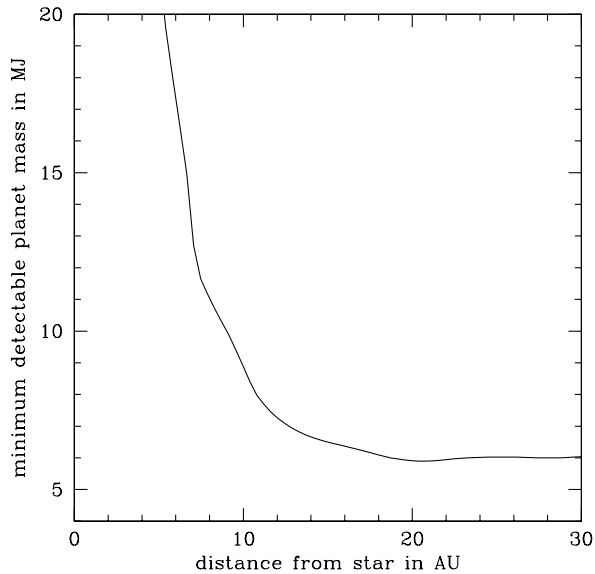


Figure 4. Mass sensitivity plot, showing the mass of the least massive planet we could detect, in units of Jupiter masses, vs projected physical separation from the star. These are realistic, 10σ limits, as confirmed by our Monte Carlo simulation.

Doug Miller and Matt Kenworthy for effectively operating their complex and sometimes finicky systems, and working with us to achieve our challenging science goals. This research has made use of the SIMBAD database, operated at CDS, Strasbourg, France. Our code for the analyses described here makes extensive use of Numerical Recipes⁵ subroutines.

REFERENCES

1. I. Baraffe, G. Chabrier, T. S. Barman, F. Allard, and P. H. Hauschildt, “Evolutionary models for cool brown dwarfs and extrasolar giant planets. the case of hd 209458,” *Astronomy and Astrophysics* **402**, pp. 701–712, 2003.
2. C. Marois, D. Lafrenière, R. Doyon, B. Macintosh, and D. Nadeau, “Angular differential imaging: A powerful high-contrast imaging technique,” *The Astrophysical Journal* **641**, pp. 556–564, 2006.
3. A. I. Galeev, I. F. Bikmaev, F. A. Musaev, and G. A. Galazutdinov, “Chemical composition of 15 photometric analogs of the sun,” *Astronomy Reports* **48**, **6**, pp. 492–510, 2004.
4. A. N. C. (editor), *Allen’s Astrophysical Quantities*, Springer-Verlag, New York, 2000 (fourth edition).
5. W. H. Press, S. A. Teukolsky, W. T. Vetterling, and B. P. Flannery, *Numerical Recipes in C*, Cambridge University Press, New York, 1992 (second edition).